






Article

Numerical Investigation of Microchannel Heat Sink with Trefoil Shape Ribs

Sadiq Ali ¹, Faraz Ahmad ^{2,*} , Kareem Akhtar ^{1,*}, Numan Habib ³, Muhammad Aamir ⁴ , Khaled Giasin ⁵ , Ana Vafadar ⁴  and Danil Yurievich Pimenov ⁶ 

¹ Department of Mechanical Engineering, University of Engineering & Technology, Peshawar 25120, Pakistan; Sadiq.ali@uetpeshawar.edu.pk

² Department of Mechanical Engineering, Aerospace and Aviation Campus, Air University Islamabad, Kamra 43570, Pakistan

³ Department of Mechanical Engineering, CECOS University of Information Technology and Emerging Sciences, Peshawar 25000, Pakistan; numanhabib@cecos.edu.pk

⁴ School of Engineering, Edith Cowan University, Joondalup, WA 6027, Australia; m.aamir@ecu.edu.au (M.A.); a.vafadarshamasbi@ecu.edu.au (A.V.)

⁵ School of Mechanical and Design Engineering, University of Portsmouth, Portsmouth PO1 3DJ, UK; khaled.giasin@port.ac.uk

⁶ Department of Automated Mechanical Engineering, South Ural State University, Lenin Prosp. 76, 454080 Chelyabinsk, Russia; danil_u@rambler.ru

* Correspondence: faraz.ahmad0460@gmail.com (F.A.); kareemakhtar@uetpeshawar.edu.pk (K.A.)

Abstract: The present study investigates the thermo-hydraulic characteristics of a microchannel sink with novel trefoil shaped ribs. The motivation for this form of rib shape is taken from the design of lung alveoli that exchange oxygen and carbon dioxide. This study has been conducted numerically by using a code from the commercially available Fluent software. The trefoil shaped ribs were mounted on the centerline of different walls of the microchannel in three different configurations. These consisted of base wall trefoil ribs (MC-BWTR), sidewall trefoil ribs (MC-SWTR), all wall trefoil ribs (MC-AWTR) and smooth channel (MC-SC) having no ribs on its wall. The streamline distance between the ribs was kept constant at 0.4 mm, and the results were compared by using pressure drop (Δp), Nusselt number (Nu), thermal resistance (R_{th}) and thermal enhancement factor (η). The results indicated that the addition of trefoil ribs to any wall improved heat transfer characteristics at the expense of an increase in the friction factor. The trends of the pressure drop and heat transfer coefficient were the same, which indicated higher values for MC-AWTR followed by MC-SWTR and a lower value for MC-BWTR. In order to compare the thermal and hydraulic performance of all the configurations simultaneously, the overall performance was quantified in terms of the thermal enhancement factor, which was higher than one in each case, except for MC-AWTR, in $100 < Re < 200$ regimes. The thermal enhancement factor in the ribbed channel was the highest for MC-SWTR followed by MC-BWTR, and it was the lowest for MC-AWTR. Moreover, the thermal enhancement factor increases with the Reynolds number (Re) for each case. This confirms that the increment in the Nusselt number with velocity is more significant than the pressure drop. The highest thermal enhancement factor of 1.6 was attained for MC-SWTR at $Re = 1000$, and the lowest value of 0.87 was achieved for MC-AWTR at $Re = 100$.

Keywords: microchannel heat sink; trefoil ribs; thermal enhancement; thermal resistance



Citation: Ali, S.; Ahmad, F.; Akhtar, K.; Habib, N.; Aamir, M.; Giasin, K.; Vafadar, A.; Pimenov, D.Y. Numerical Investigation of Microchannel Heat Sink with Trefoil Shape Ribs. *Energies* **2021**, *14*, 6764. <https://doi.org/10.3390/en14206764>

Academic Editors: Dimitris Drikakis and Pouyan Talebizadeh Sardari

Received: 9 September 2021

Accepted: 14 October 2021

Published: 17 October 2021

Publisher's Note: MDPI stays neutral with regard to jurisdictional claims in published maps and institutional affiliations.



Copyright: © 2021 by the authors. Licensee MDPI, Basel, Switzerland. This article is an open access article distributed under the terms and conditions of the Creative Commons Attribution (CC BY) license (<https://creativecommons.org/licenses/by/4.0/>).

1. Introduction

The increasing demand for digitalization has shifted the trend of the modern world towards the miniaturization of electronic equipment where hundreds of thousands of transistors are installed on a single silicon chip. Due to the reduction in the sizes of these equipment, the power density increased rapidly and can be as high as up to 1 W/mm^2 . However, great care is needed to maintain such equipment for its safety and improved

life cycle. Therefore, modern techniques including cooling using liquid such as a micro-jet, heat pipe, spray impingement and microchannel cooling are introduced to fulfill the requirement of higher heat dissipation [1]. Over time, the cooling techniques have been improved from cooling by force convection and air to more advanced techniques.

The microchannel cooling system was first coined in 1981 by Tuckerman and Pease [2]. Microchannel cooling is a passive technique for dissipating heat from electronic devices without occupying a larger space than other dissipating setups. A microchannel heat sink (MCHS) with smooth geometry is used to dissipate heat from different devices. The usage and capacity of microelectronic equipment increased drastically; as a result, an increased amount of heat is produced inside this equipment. To dissipate this large amount of heat, a smooth MCHS will be unable for that much dissipation. Therefore, the thermal performance of smooth MCHS needs improvement. The thermal performance of MCHS can be improved by performing some modifications to the smooth one and then some thermal performance parameters such as thermal enhancement factor (η), friction factor (f) and Nusselt number (Nu) will be compared with a smooth channel after modification (adding some extended surfaces or cavities) to the channel. In most cases, the better thermal performance of MCHS is associated with irreversibility in the flow field, which is computed in terms of friction factor (f), entropy generation (S_{gen}) and thermal resistance (R_{th}). The main objective of many researchers is to increase the heat dissipation rate (Nusselt number (Nu)) with minimal pressure loss [3–6].

Many researchers worked on the effect of extended surfaces (fins or ribs) on the performance improvement of MCHS. For example, Rehman et al. [7] added dimple shaped ribs to the smooth channel for enhancement in the overall performance of the smooth channel. In their study, different cases were used, which included base wall ribs, sidewall ribs and all walls' ribs. Moreover, aligned, staggered and mixed configurations of each case were investigated numerically. Their results concluded that the case in which all walls were ribbed had better overall performance for each configuration. The worst performance was noted for the case in which ribs were added to the sidewall. Similarly, numerical studies and comparisons of heat transfer, friction factor and thermal enhancement factor of six different micro-channels were carried out by Zhu et al. [8], and they intended to report the best one. The study compared smooth rectangular micro-channel, side grooved rectangular micro-channel, side grooved with diamond shape ribs, side grooved with rectangular shape ribs, side grooved with elliptic shape ribs and side grooved with forwarding triangular shape ribs micro-channel. The results concluded that the combination of grooves and ribs has better performance than simple ribbed micro-channel. The side grooved with rectangular shape ribs micro-channel has the best overall performance at $Re = 500$, relative rib width = 0.25 mm and minimum rib-groove distance = 0.1 mm.

Xiao et al. [9] worked on the thermal improvement of micro-channel by producing turbulence in a flow field with the help of V-shape ribs. A significant enhancement in the overall performance of micro-channel has been noted from this numerical study. Similarly, Hassani et al. [10] conducted a numerical and experimental study to investigate the enhancement in the overall performance of MCHS by adding pins and chamber shape cavity to it. In their study, four different cases were used, which included smooth micro-channel, smooth micro-channel with pins, smooth micro-channel with chamber shape cavity and smooth micro-channel with pins and chamber shape cavity. Their results concluded that the addition of pins improved heat transfer by 44.8% and chamber shape cavity by 3.7%, while the simultaneous addition of pins and cavity improved heat transfer by 37.5%. The highest enhancement factor was noted for the pin located at the middle of the cavity. Furthermore, Ahmad et al. [11] used cylindrical shape ribs and cavities to numerically investigate the performance enhancement in MCHS with different cases. In this study, a base wall with cylindrical shape ribs, a sidewall with cylindrical shape ribs and all walls with cylindrical shape ribs were compared. Moreover, the effects of rib spacing for all wall ribs cases and comparisons of all wall ribs, all wall cavities and the combination of both were also taken into account in this study. It was concluded that the case of all wall

ribs performed best among all cases, based on entropy generation, thermal enhancement factor, thermal resistance and transport efficiency.

Yang et al. [12] proposed three different pin fin cross sections attached to micro-channel heat sinks to improve heat dissipation capacity. These cross-sections include rhombus, hydrofoil and sinusoidal shapes. Their experimental and numerical results concluded that the performance of the sinusoidal cross section performed best among the three cases compared. Similarly, Naquiuddin et al. [13] studied the effects of structure parameters on rectangular micro-channel and found that for any structure, the performance in terms of heat transfer increases at the cost of higher pressure drop. The average temperature of the channel was reduced by 33 K with an increase of 1000 kPa pressure drop. The optimum performance was noted for the coolant's flow rate of less than 200 mL/min. Similarly, Wang et al. [14] carried a numerical study of rectangular micro-channel with sidewall truncated ribs. Three different ribs parameters, including truncation gap height, width and ribs arrangement, were used to study the improvement in the hydro-thermal behavior of MCHS in flow regimes of $100 < Re < 1000$. Their study confirmed that the results of truncated ribs are far better than their counterpart traditional ribs; the parallel arrangement results in a higher overall heat transfer coefficient.

Chuan et al. [15] used porous ribs instead of solid ribs with a straight channel to assess the performance of the micro-channel. They examined that, with porous ribs, the increment in pressure drop is lower than compared to solid ribs of exact dimensions. Moreover, the same porous rib increased the thermal resistance at the same time. Similarly, Wang et al. [16] proposed a multi-objective genetic optimization technique for the optimal design of MCHS. In their study, double-layered MCHS with semi-porous ribs was considered. It was concluded that the decrement in thermal resistance is linked with an increment in pumping power. For an optimum design, pumping power is reduced by 16.40% and thermal resistance by 14.06% compared to the reference design. Furthermore, Ahmad et al. [17] proposed four different novel shapes of ribs attached to the sidewall of rectangular microchannel heat sinks, including trapezoidal, rectangular, elliptical and hydrofoil shapes for the improvement of the hydro-thermal performance of MCHS. The results revealed that each case improved overall heat transfer performance. Moreover, elliptical ribs have better thermal performance; however, the hydrofoil file has better performance in terms of friction factor and pressure loss.

Keeping in view the above literature, it is very obvious that the addition of each type of ribs enhances heat transfer with an increase in pumping power. Considerable research has been performed on traditional shapes of ribs; however, no significant work was found on unique shape ribs. In this study, bio-inspired rib shape (trefoil) is used where ribs are added in three different wall configurations consisting of ribs added to the base wall (BWTR), Sidewall (SWTR) and (AWTR). The addition of trefoil shape ribs is expected to significantly improve the overall performance of MCHS. The novelty of this work is due to the unique bio-inspired shape of ribs, and the motivation is basically taken from the lungs of humans; the lung's internal structure consists of trefoils such as shape alveoli which are involved in the exchange of oxygen and carbon dioxide.

The present study aims to investigate the performance of MCHS numerically with novel trefoil ribs using ANSYS Fluent. This study aims to analyze the performance of MCHS by employing a novel shaped rib at different walls. The proposed models of novel ribs include trefoil shape ribs. The use of trefoil rib is the special novelty of this study, and it has not been investigated in the past literature. In most of the previous papers, the ribs were mounted on the sidewalls of MCHS in the transverse configuration. However, in this study, the ribs were mounted in the centerline configuration and mounted on different walls, i.e., base wall, sidewall and all walls. This study assesses the performance of MCHS with trefoil shape ribs by using numerical simulation in a laminar flow regime with Reynolds number (Re) in the range of 10–1000. Moreover, the performance of the base wall with trefoil ribs (BWTR), sidewall with trefoil ribs (SWTR) and all walls with trefoil ribs (AWTR) was compared with each other and with smooth micro-channel based

on thermal resistance, pressure drop, friction factor ratio, heat transfer coefficient, Nusselt number ratio and thermal enhancement factor.

2. Materials and Methods

In the present study, the micro-channel is made of copper, and water is used as a coolant. Numerical simulations of the microchannel (3D) using CFD techniques (RANS Simulations) are analyzed. During numerical simulations, the smooth micro-channel and micro-channel with trefoil shape ribs attached to the centerline of base, side and to all walls with a streamline distance of 0.4 mm were modelled. The model was meshed and imported to CFD Fluent in order to calculate Δp , h , f/f_0 , Nu/Nu_0 , R_{th} and η with the addition of trefoil shape ribs. The details of the material used and methodology adopted for the present study are given in the following section respectfully.

2.1. Geometrical Shape of MCHS

In the present study, a rectangular microchannel is used because of its superior thermal performance among circular, hexagonal, rectangular and triangular cross-sections [18]. Ribs in the trefoil shape are attached to the base wall, sidewall and all walls with a stream-wise distance (pitch) of 0.4 mm; the computational domain of each case and geometric details of the trefoil rib are shown in Figure 1. Moreover, the thermophysical properties of both the fluid (water) and solid (copper) domains are kept constant and are given in Table 1.

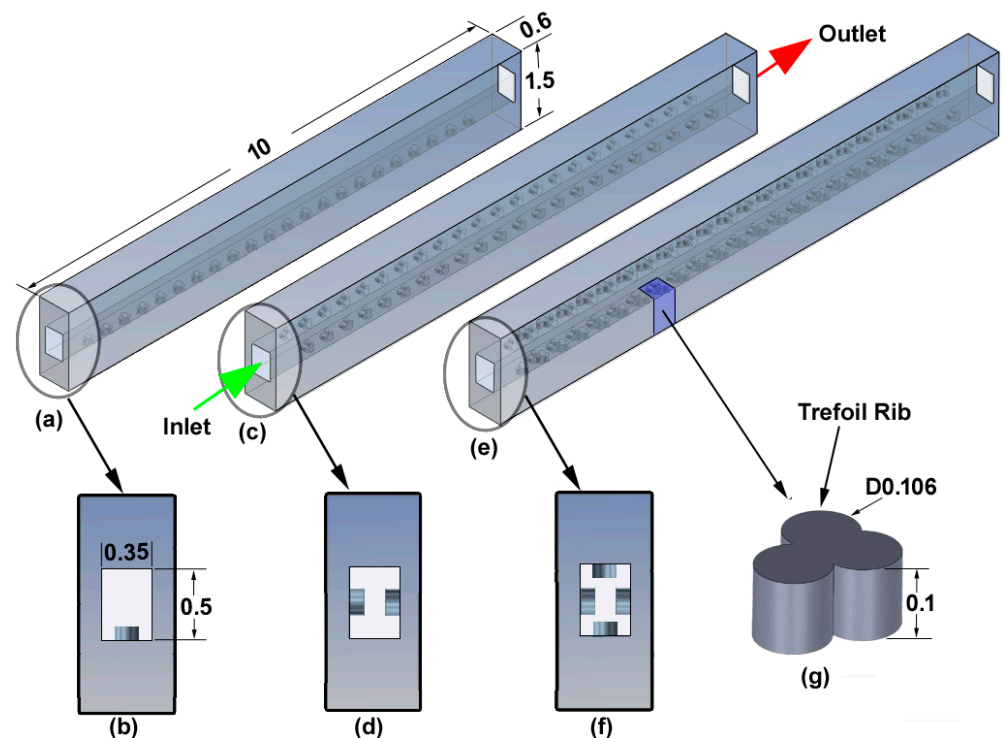


Figure 1. Computational domain of (a,b) MC-BWTR, (c,d) MC-SWTR, (e,f) MC-AWTR and (g) geometric details of trefoil rib.

Table 1. Thermophysical properties of materials.

	ρ (kg/m ³)	C_p (/kg/K)	k (W/m/K)	μ (kg/m/s)
Copper	8978	381	387.6	
Water	998.2	4812	0.6	0.001003

2.2. Governing Equations

The fluid is a Newtonian fluid with constant thermophysical properties, and the flow is laminar, steady-state and incompressible. Moreover, the effects of radiation and body forces are negligible and can be neglected. With all these assumptions, the governing equations for solid as well as a fluid domain can be presented as follows:

Continuity equation for fluid:

$$\frac{\partial u}{\partial x} + \frac{\partial v}{\partial y} + \frac{\partial w}{\partial z} = 0 \quad (1)$$

where u , v and w are the velocity component of fluid in the x , y and z directions, respectively. The movement equations in x -direction, y -direction and z -direction are written as stated below:

$$u \frac{\partial u}{\partial x} + v \frac{\partial u}{\partial y} + w \frac{\partial u}{\partial z} = -\frac{1}{\rho_f} \frac{\partial p}{\partial x} + \frac{\mu_f}{\rho_f} \left(\frac{\partial^2 u}{\partial x^2} + \frac{\partial^2 u}{\partial y^2} + \frac{\partial^2 u}{\partial z^2} \right) \quad (2)$$

$$u \frac{\partial v}{\partial x} + v \frac{\partial v}{\partial y} + w \frac{\partial v}{\partial z} = -\frac{1}{\rho_f} \frac{\partial p}{\partial y} + \frac{\mu_f}{\rho_f} \left(\frac{\partial^2 v}{\partial x^2} + \frac{\partial^2 v}{\partial y^2} + \frac{\partial^2 v}{\partial z^2} \right) \quad (3)$$

$$u \frac{\partial w}{\partial x} + v \frac{\partial w}{\partial y} + w \frac{\partial w}{\partial z} = -\frac{1}{\rho_f} \frac{\partial p}{\partial z} + \frac{\mu_f}{\rho_f} \left(\frac{\partial^2 w}{\partial x^2} + \frac{\partial^2 w}{\partial y^2} + \frac{\partial^2 w}{\partial z^2} \right) \quad (4)$$

where ρ_f represents the density, and μ_f is the dynamic viscosity of the working fluid.

The energy equation for fluid and solid domains can be written as follows:

$$u \frac{\partial T_f}{\partial x} + v \frac{\partial T_f}{\partial y} + w \frac{\partial T_f}{\partial z} = \frac{k_f}{\rho_f C_{p_f}} \left(\frac{\partial^2 T_f}{\partial x^2} + \frac{\partial^2 T_f}{\partial y^2} + \frac{\partial^2 T_f}{\partial z^2} \right) \quad (5)$$

$$k_s \left(\frac{\partial^2 T_s}{\partial x^2} + \frac{\partial^2 T_s}{\partial y^2} + \frac{\partial^2 T_s}{\partial z^2} \right) = 0 \quad (6)$$

where T_f is the fluid temperature, k_f is the thermal conductivity and C_{p_f} is the specific heat of the working fluid. T_s is the temperature, and k_s is the thermal conductivity of the solid domain.

The following boundary conditions were used to solve the above equations.

At the inlet of the channel where $x = 0$ mm, the velocity-inlet boundary conditions with a fluid inlet temperature of 293.15 K are assumed to be as follows.

$$u = u_{in} \quad (7)$$

$$T_f = T_{in} \quad (8)$$

The different values for u_{in} are calculated by using an Re number in the range of 100 to 1000.

At the outlet of the channel, where $x = 10$ mm, we have the following.

$$p = p_{out} = 1 \text{ atm} \quad (9)$$

At the bottom surface, the uniform heat flux is given by the following.

$$q = 100 \frac{w}{cm^2} \quad (10)$$

At inner wall of the channel, no slip boundary conditions are applied as follows.

$$u = v = w = 0 \quad (11)$$

$$-k_s \frac{\partial T_s}{\partial n} = -k_f \frac{\partial T_f}{\partial n} \quad (12)$$

At all the remaining walls, the adiabatic conditions are used as follows.

$$\frac{\partial T_s}{\partial y} = \frac{\partial T_s}{\partial z} = 0 \quad (13)$$

2.3. Numerical Method and Mesh Independence

ANSYS Fluent is utilized for the numerical solution in the present study. The second-order difference schemes for discretization of diffusion terms and second-order upwind schemes for convection term are used in the present case. The convergence criteria of 10^{-6} are used for all variables. Different mesh sizes for the MC-BWT case for $Re = 500$ are solved, and the relative error in Δp and Nu is calculated to check the reliability of the solution and summarized in Table 2:

$$e\% = \frac{P_2 - P_1}{P_1} * 100 \quad (14)$$

where P_1 is the value of any parameter with the smallest mesh size, and P_2 is the value with other mesh sizes.

Table 2. Mesh independence test.

Mesh No	No of Elements	Pressure Drop (Pa)	Error (%)	Nu	Error (%)
1	568,956	4342.478	0.58	11.68255	0.83
2	691,194	4350.475	0.34	11.65281	0.58
3	811,646	4360.415	0.17	11.63914	0.46
4	963,976	4366.139	0.038	11.65263	0.058
5	1,231,560	4367.813		11.58557	

As shown in Table 2, for Mesh No. 3, the relative error in pressure was less than 0.2%, and the relative error in Nu was less than 0.5%; thus, this mesh, with 811,646 number of elements, was used for analysis in the present study.

2.4. Data Reduction

In MCHS, the η is used for performance measurement of different micro-channels; it is a function of both ratios of Nu and f and is given by the following equation [19].

$$\eta = \frac{(Nu/Nu_0)}{(Nu/Nu_0)^{\frac{1}{3}}} \quad (15)$$

In this equation, f is the Darcy friction factor [20], and Nu is the Nusselt number given by the following:

$$f = \frac{2D_h \Delta p}{L_{ch} \rho_f u_m^2} \quad (16)$$

$$Nu = \frac{h_{avg} D_h}{k_f} \quad (17)$$

where D_h is the hydraulic diameter, Δp is the pressure drop, L_{ch} is the length of the channel and h_{avg} is the average heat transfer coefficient and can be calculated by following relationships:

$$D_h = \frac{2H_{ch}W_{ch}}{H_{ch} + W_{ch}} \quad (18)$$

$$h_{avg} = \frac{q_w A_{base}}{2(W_{ch} + H_{ch})L_{ch}\Delta T} \quad (19)$$

where H_{ch} is the height, W_{ch} is the width of the channel, q_w is the heat flux and A_{base} is the area of the base wall. ΔT is the temperature difference between channel wall temperature (T_w) and fluid mean temperature (T_f), and they are given by the following.

$$\Delta T = T_w - T_f \quad (20)$$

$$T_w = \frac{\int T_{w-x,y} dy dx}{\int dy dx} \quad (21)$$

$$T_b = \frac{\int T_{b-x,y} dy dx}{\int dy dx} \quad (22)$$

$$T_f = \frac{\int T_{f-i,x} \rho_{f-i,x} \left| \vec{v} \cdot \vec{dA} \right| dx}{\int \rho_{f-i,x} \left| \vec{v} \cdot \vec{dA} \right| dx} \quad (23)$$

The overall thermal resistance is given as follows.

$$R_{tot} = R_{cond} + R_{conv} + R_{cap} \quad (24)$$

$$R_{tot} = \frac{T_b - T_{ch}}{q_w A_b} + \frac{T_{ch} - T_f}{q_w A_b} + \frac{T_f - T_{in}}{q_w A_b} = \frac{T_b - T_{in}}{q_w A_b} \quad (25)$$

3. Results

The accuracy of numerical schemes used for the present study is first validated with available experimental work in literature. The validated numerical modal is then used for calculating the Δp , h , f/f_0 , Nu/Nu_0 , R_{th} and η for MC-BWTR, MC-SWTR and MC-AWTR. The calculated values for ribbed channels are compared with the reference case (MC-SC), which are discussed in detail in the following sections.

3.1. Model Validation

As shown in Figure 2, the Nu and f values were calculated and compared to the experimental work of Wang et al. [21] with the uniform inlet velocity, $T_{in} = 293$ K, which is calculated from Re and a heat flux of 100 W/cm^2 with the same conditions as used in the experimental study [21]. The obtained results were close to the experimental results available in the literature with less than 5% deviation; hence, the present model can be used for calculating the thermal-hydraulic perimeters of MCHS.

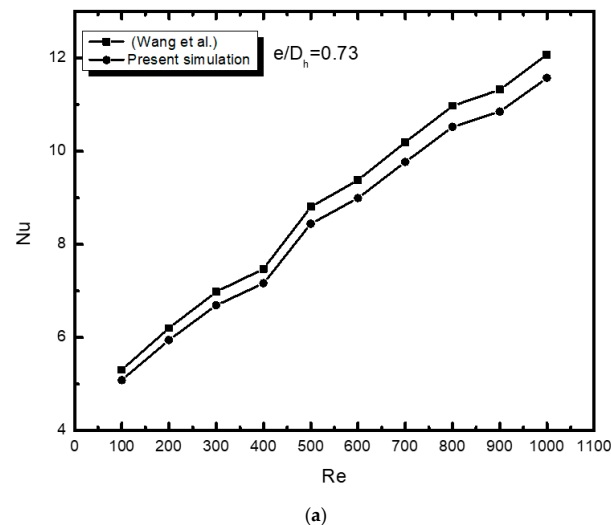


Figure 2. Cont.

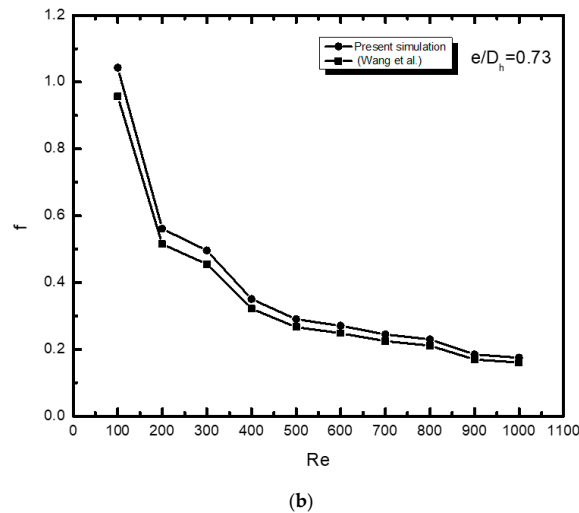


Figure 2. Validation of (a) Nusselt number and (b) friction factor with Wang et al. [21].

3.2. Characteristics of Temperature and Pressure Distribution

The temperature distribution for MCHS with trefoil shaped ribs was added to the base wall (BWTR), sidewall (SWTR) and all wall (AWTR) cases together with the smooth channel, which is shown in Figure 3. This was performed in order to study the temperature distribution (cooling) with the addition of trefoil shape ribs. MC-AWTR case showed better cooling in terms of temperature drop followed by MC-SWTR and MC-BWTR, respectively.

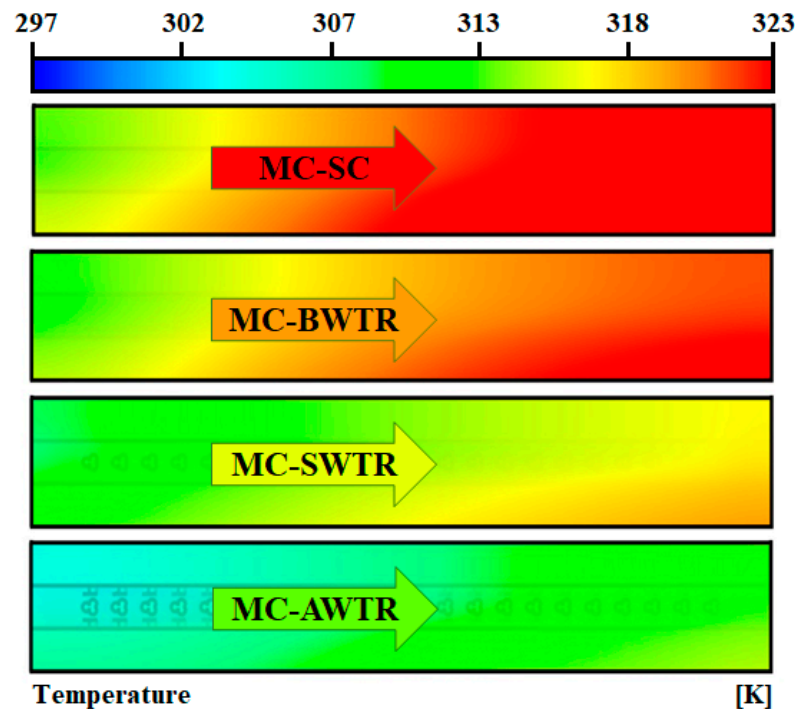


Figure 3. Temperature distribution of MCHS with trefoil shaped ribs attached to different walls.

The increase in thermal performance was at the cost of an increase in power required to pump the same amount of fluid because the ribs blocked the flow and increased the pressure requirement. The pressure distribution was the determining factor for pumping power; the pressure distributions of all ribbed cases along with smooth channel are presented in Figure 4. The pressure drop in the smooth channel was due to the friction of the wall, while for the ribbed channel, it was the combined effect of wall roughness and resistance offered

to the flow by ribs. The pressure drop of MC-SC is minimum, and the pressure drop for MC-AWTR is highest because of the presence of a higher number of ribs.

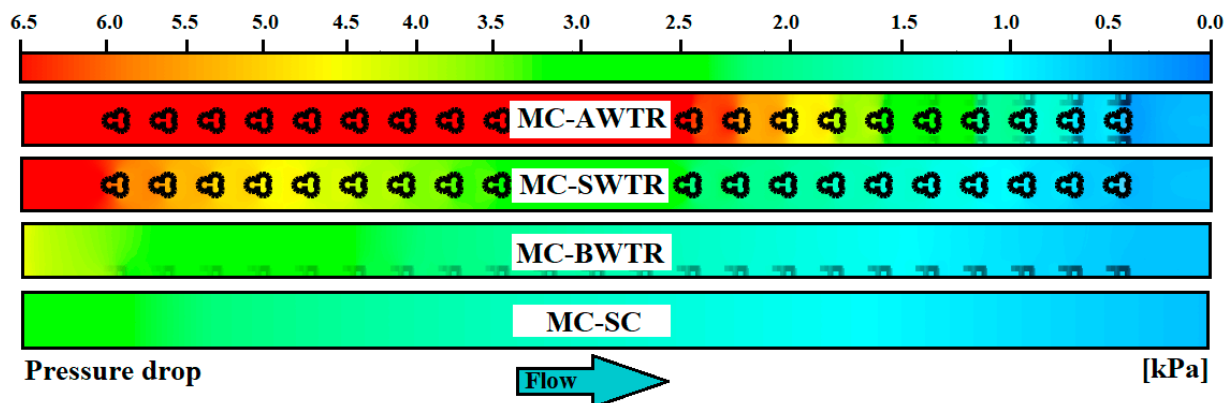


Figure 4. Pressure distribution of MCHS with trefoil shape ribs attached to different walls.

The temperature distribution (cooling diagram) recommended the MC-AWTR case, while the pressure distribution recommended MC-BWTR. Other performance parameters can be analyzed for final conclusions.

3.3. Performance Comparison

Performance measurement of all cases was carried out for $Re = 100\text{--}1000$ with a step of 100, and the results are presented in contrasting graphs to indicate the improvements made by the trefoil shaped ribs. In addition to the performance improvements in the different cases and the reference case, MC-SCs were compared by plotting Δp , h , f/f_0 , Nu/Nu_0 , R_{th} and η .

The Δp of the MCHS with trefoil shaped ribs and a straight channel are displayed in Figure 5. The lowest Δp was attained in the MC-SC case, which was only produced by the wall's roughness. The Δp in the ribbed channel cases, MC-BWTR, MC-SWTR and MC-AWTR, was a combination of Δp by the wall's roughness and Δp produced by the blockage offered by ribs. The Δp for the MC-BWTR case was minimal compared with the other ribbed cases, and this was due to the ribs being attached to only one wall. However, in the MC-SWTR and MC-AWTR cases, the ribs were attached to either two or four walls, respectively. In the MC-SWTR case, the ribs were attached to two walls; therefore, the number of ribs, in this case, was higher than for MC-BWTR. As such, the Δp was more than the MC-SC and MC-BWTR cases. A maximum Δp was noted for the MC-AWTR case because each wall contained ribs and blocked the flow, thereby causing the Δp to rise. At $Re < 250$, the Δp for MC-SC, MC-BWTR and MC-SWTR was almost the same, whereas the MC-AWTR case displayed higher Δp . Moreover, in the range of $100 < Re < 600$, the MC-BWTR Δp was almost equal to MC-SC compared to Δp in the other cases, which was significantly higher. The pressure drop increases with an increase in Re for all cases; however, this increase is minimal in the low Re range, while the increase is maximal in the higher Re range, i.e., $Re > 500$. Moreover, the pressure drop behaviour against Re of MC-AWTR is stiffer when compared to other ribbed cases such as MC-SWTR and MC-BWTR, which is flattened and indicates that the increase in Δp for MC-AWTR case is higher than MC-SWTR and MC-BWTR.

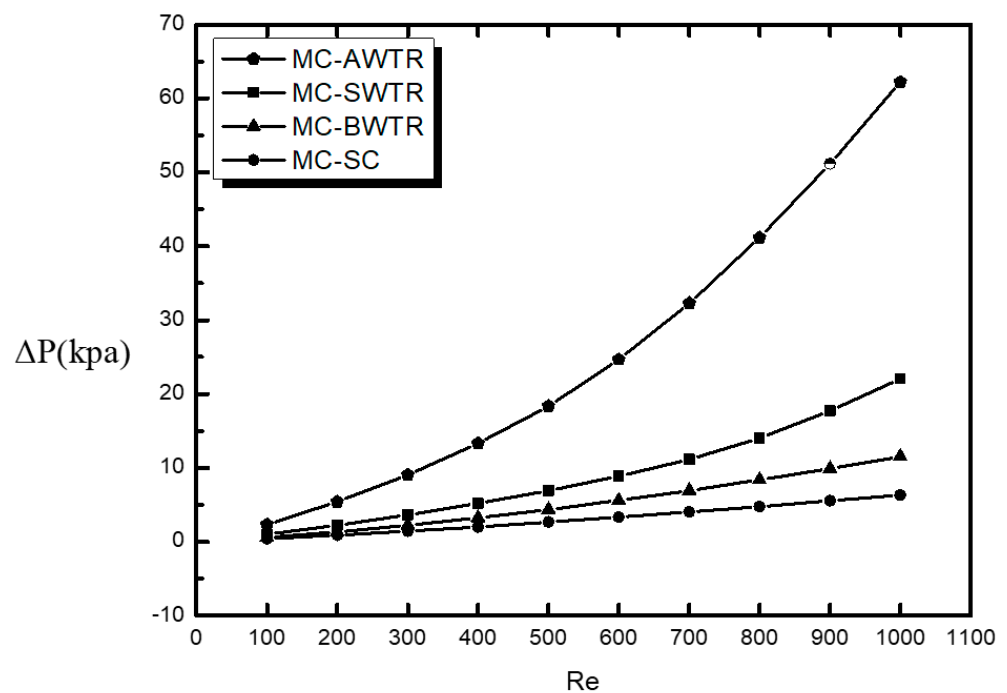


Figure 5. Comparison of pressure drop for various wall configurations MCHS.

Figure 6 shows the comparison of h for the various MCHSs together with the MC-SC. It is clear that the h value in all ribbed cases was significantly higher than for the MC-SC. The addition of trefoil shaped ribs caused better mixing and produced higher h values as a result. The heat transfer coefficient for the MC-AWTR case was highest, and it was the lowest for MC-BWTR. This could be because the number of ribs in MC-AWTR is greater than that of MC-BWTR, which provides more heat transfer area and better mixing of fluid. Moreover, the MC-SWTR case had better performance in terms of heat transfer than the MC-SC and MC-BWTR cases. The increase in h at $Re < 200$ from MC-SC to the ribbed channel was smaller; however, at $Re > 200$, the increase was significantly higher because the turbulence was higher at Re , which caused high heat transfer. Furthermore, h increases with an increase in Re . The highest increase is noted for each case compared to the straight channel (MC-SC) at $Re = 1000$, which is 3, 2.4 and 1.7 times for MC-AWTR, MC-SWTR and MC-BWTR, respectively.

The friction caused by the addition of ribs to the base wall, sidewalls and all walls resulted in an increase in friction factor. The relative increase in friction factor with trefoil shaped ribs was calculated in terms of friction factor ratio (f/f_0) and plotted against Re , as shown in Figure 7. It is clear that the f/f_0 for MC-BWTR and MC-SWTR was considerably smaller than the ratio for MC-AWTR. The f/f_0 at $Re = 1000$ for MC-AWTR and MC-SWTR is 1.9 and 5.39 times higher when compared to MC-BWTR, respectively, because the friction factor is the measure of the resistance to flow, which is at the maximum in the case of the low flow area of MC-AWTR. The f/f_0 ratio rose with the increase in Re , while an increase in the SC-BWTR case was almost negligible, as indicated by the flatness of the curve. This was because very few turbulence enhancers were present at the base wall. The increase in the f/f_0 for MC-SWTR with an increase in the Re was insignificant up to $Re < 700$ regimes; however, the increase was significant above $Re > 700$ regimes for the MC-AWTR case. The f/f_0 rose with the increase in Re number throughout due to the presence of ribs at all walls.

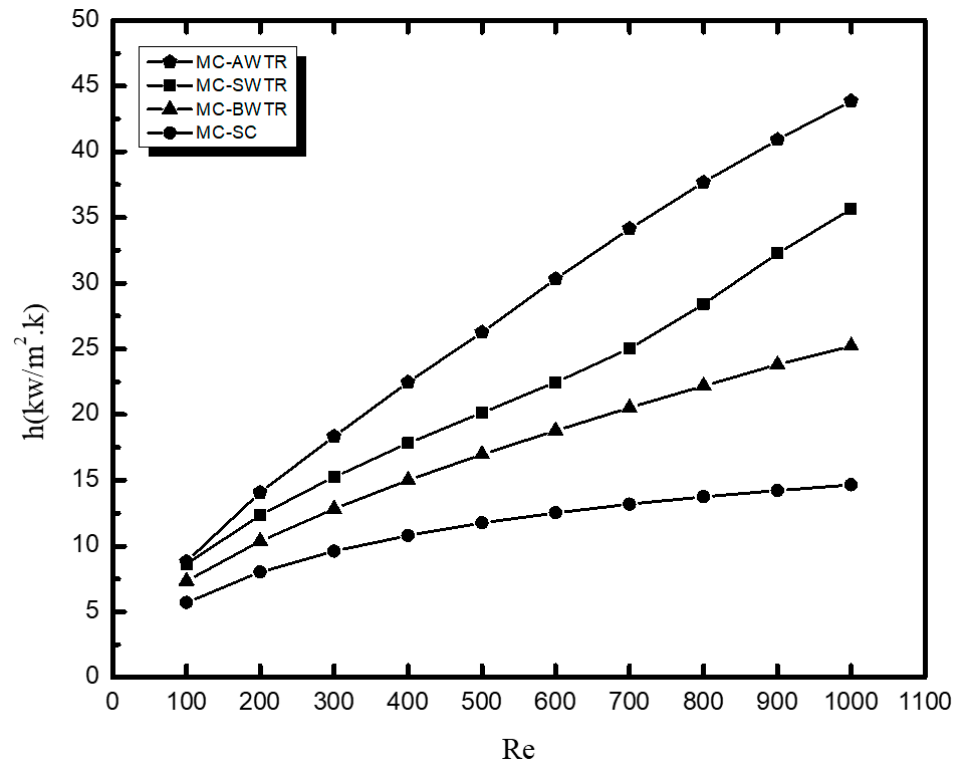


Figure 6. Comparison of heat transfer coefficient for different wall configurations of MCHS.

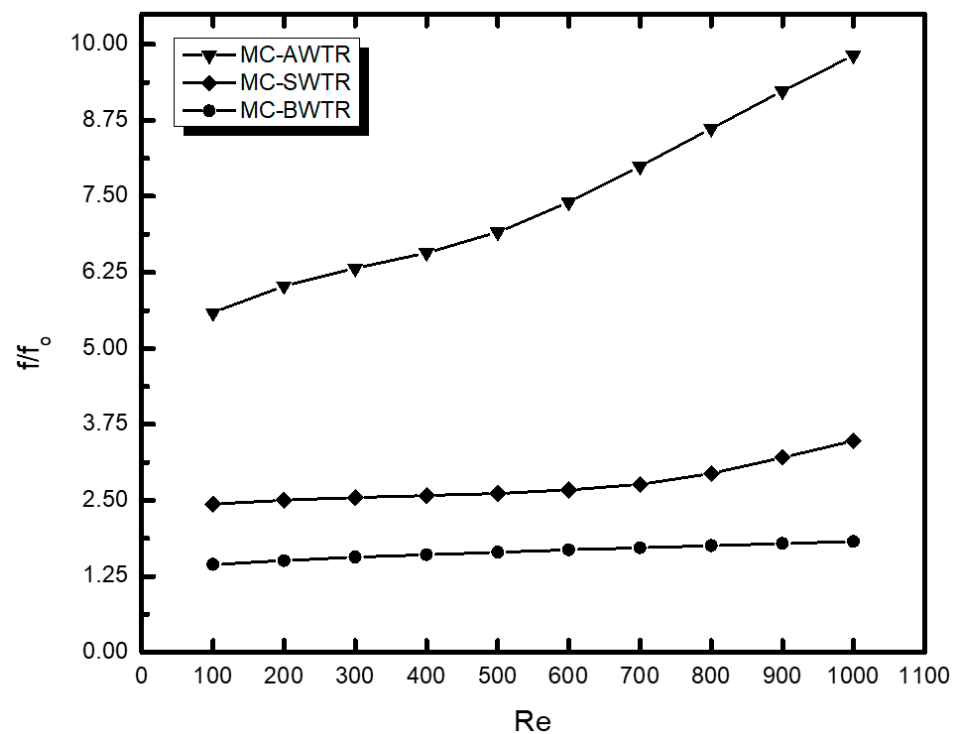


Figure 7. Comparison of friction factor ratio for different wall configurations MCHS.

Figure 8 shows the comparison of the Nu for various MCHSs along with the MC-SC. The Nu is a dimensionless number used to indicate the capability of heat transfer by a channel. The higher the Nu number, the more effective heat transfer will be. Figure 8 indicates that the minimum value of Nu was observed for MC-SC, while the maximum value was noted for MC-AWTR. Conversely, MC-BWTR had a smaller Nu than MC-SWTR

and MC-AWTR. The average percentage increase in Nu is 142%, 90% and 51% for MC-AWTR, MC-SWTR and MC-BWTR, respectively, when compared to MC-SC. The Nu was directly proportional to the effective heat transfer area, which was maximum for MC-AWTR and minimum for MC-SC. The effective heat transfer area for MC-SWTR was higher than MC-BWTR, and this explained why MC-SWTR performed better in terms of Nu than MC-BWTR. Moreover, Nu inclined linearly with Re for all cases except MC-SWTR after $Re > 600$. This was because the ribs were attached to both sides in MC-SWTR, which produced turbulence compared to other cases at higher velocity.

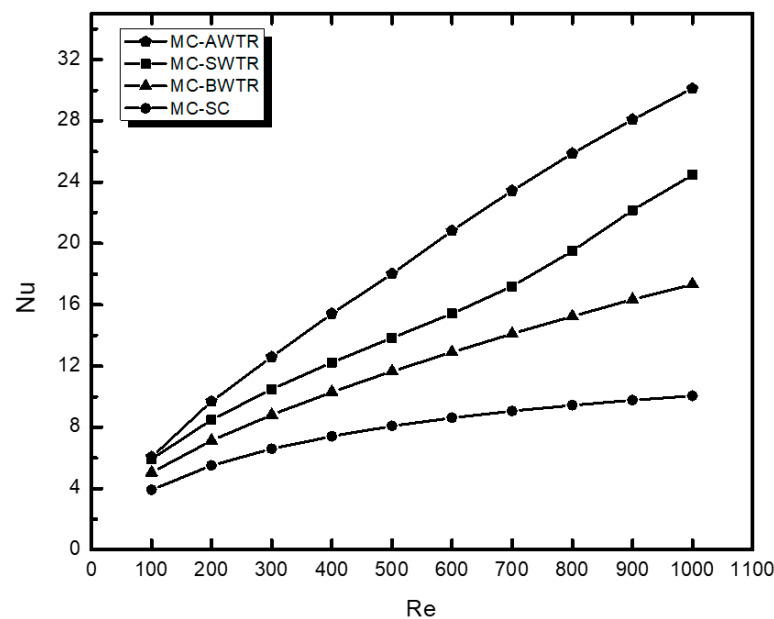


Figure 8. Comparison of Nusselt number for different wall configurations MCHS.

In order to compare the effectiveness of the heat transfer among ribbed channels, the Nu/Nu_0 of the ribbed channel and the MC-SC was plotted against the Re, and the results are presented in Figure 9. It is evident that MC-AWTR performed exceptionally well in comparison to the MC-SC in terms of Nu; the performance of MC-AWTR was three times superior to MC-SC at $Re = 1000$. MC-BWTR had a slight increase in Nu compared to MC-SC: the maximum value of Nu/Nu_0 is 1.5 at $Re = 1000$, half of the MC-AWTR at the same Re. MC-SWTR performance in terms of Nu ratio was better than MC-BWTR and slightly lower than MC-AWTR; therefore, this case's performance was 2.5 times higher than the MC-SC at $Re = 1000$. The value of Nu/Nu_0 increased smoothly with Reynolds number except for MC-SWTR in $Re > 600$. The increase in the value of Nu/Nu_0 was higher with Re and MC-BWTR in $Re < 200$, where the curve was nearly flat, representing a minor increase in Nu/Nu_0 with Re.

MCHS performed better thermally with the addition of ribs to any wall; however, the addition of ribs declined the hydrodynamic performance by increasing pressure drop, which was not required. As a result, there should be a trade-off between thermal improvement and pressure drop, which could be calculated in terms of overall η . The η for trefoil shaped ribs of different wall configuration MCHS was plotted against the Re number and is presented in Figure 10. It was clear that MC-SWTR had a higher value of η among all cases for any Re, although its heat transfer was less than MC-AWTR; however, its Δp was quite low, making the η high. The η for MC-AWTR was lowest among all cases; the increase in Nusselt number for this configuration is associated with a higher Δp , making the value of η the lowest. The value of η for MC-BWTR was higher than MC-AWTR and lower than MC-SWTR. Figure 10 shows that the value of η for all cases was higher than one except for MC-AWTR in $Re < 200$ in which the increase in Nu did not compensate for the increase in Δp . Moreover, the value of η increased in increment in Re for each

case, which confirms that the increment in Nu was more significant than the increment in Δp . The highest η value of 1.6 was attained for MC-SWTR at $Re = 1000$, whereas the lowest value of 0.87 was achieved for MC-AWTR at $Re = 100$. The thermal enhancement for MC-BWTR and MC-AWTR was almost the same in $700 < Re < 900$. The increase in η with Re for MC-BWTR was nearly uniform throughout. By contrast, MC-SWTR and MC-AWTR were non-uniform. For MC-AWTR, the η increase was more significant at $Re < 700$ and less effective at $Re > 700$ because the increase in Δp was very high than compared to Nu . For MC-SWTR in $Re > 700$ regimes, the increase in η was more rapid with Re , indicating that the increment in Nu at high Re was more significant than the increment in Δp for sidewall trefoil ribs.

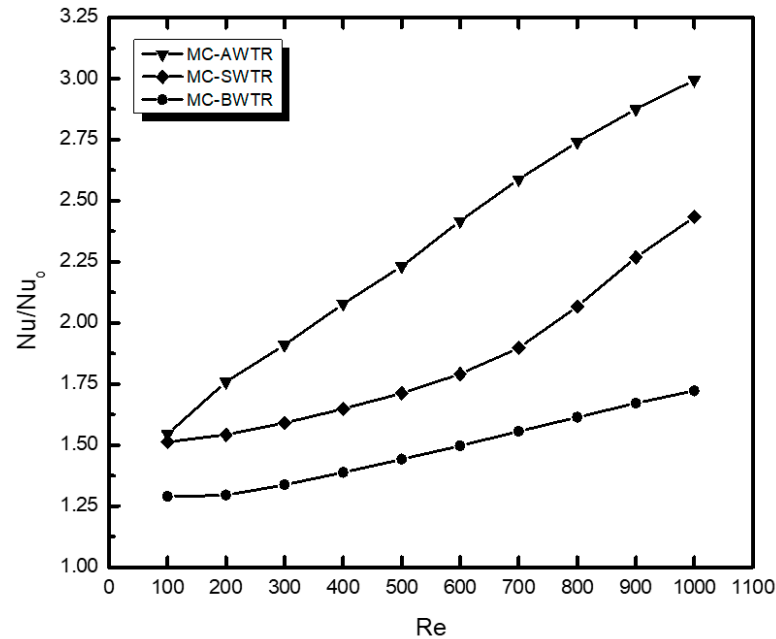


Figure 9. Comparison of Nusselt number ratio for different wall configurations MCHS.

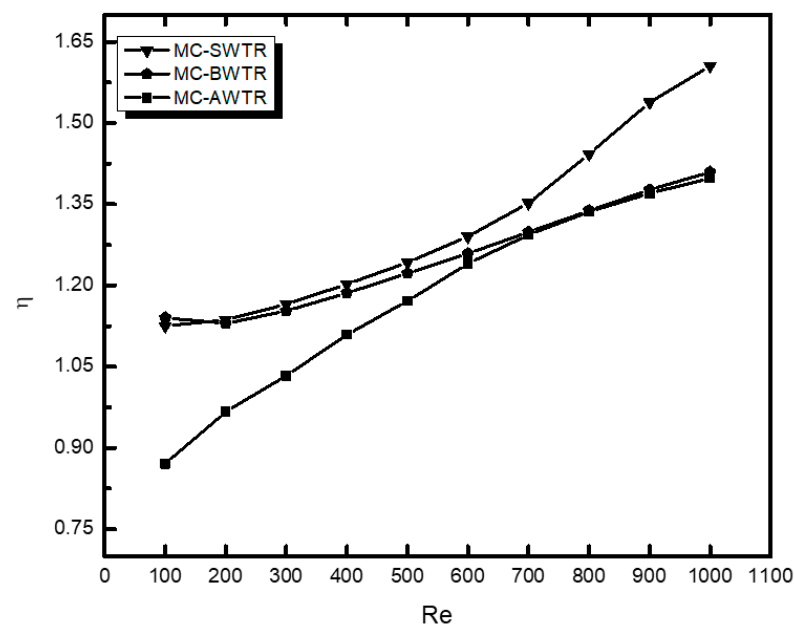


Figure 10. Comparison of thermal enhancement factor for different wall configurations MCHS.

Figure 11 shows the total R_{th} for various ribbed channel configurations against Re in a range of 100–1000. Total R_{th} demonstrates the capability of the micro-channel to transfer

heat with given pumping power. The higher the value R_{th} is, the lower the heat transfer will be with respect to pumping power. MC-SC had a higher value than any other ribbed case confirming the evidence based on the η : The performance of each ribbed case was better than the MC-SC. MC-AWTR had minimum R_{th} compared to MC-BWTR, which had maximum values among ribbed channels; however, MC-SWTR had the highest η , and its R_{th} was more elevated than MC-AWTR due to the low number of ribs that caused lower heat transfer for the same power in MC-SWTR.

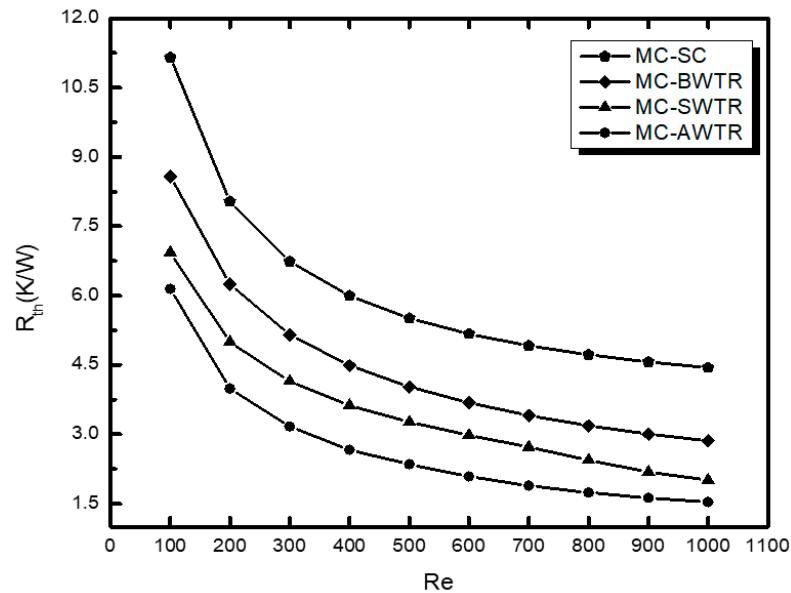


Figure 11. Comparison of total thermal resistance for different wall configurations MCHS.

4. Conclusions

In this study, the bio-inspired rib shape (trefoil) is used where ribs are added in three different wall configurations consisting of ribs added to the base wall (BWTR), Sidewall (SWTR) and (AWTR). The addition of trefoil shaped ribs significantly improved the overall performance of MCHS. The novelty of this work is due to the unique bio-inspired shape of the rib, which is basically taken from lungs of human, and the lung's internal structure consists of trefoils-like shaped alveoli that are actually involved in the exchange of oxygen and carbon dioxide.

The present study utilizes the Fluent code to investigate the heat transfer and flow field of MCHS with trefoil shaped ribs. The trefoil shaped ribs in this study were mounted to the center of the base wall, sidewall and all walls with a streamline distance of 0.4 mm. The performance improvement has been calculated in terms of Δp , h , f , Nu , R_{th} and η for Reynolds number in the range of $Re = 100$ to $Re = 1000$. Based on the results discussed in the present study, the following significant points are concluded as follows:

- The addition of trefoil ribs to any wall improved heat transfer characteristic (h and Nu) of MC-SC; the improvement was greater in MC-AWTR followed by MC-SWTR and minimum for MC-BWTR.
- The addition of ribs to any wall has increased the friction factor and, hence, the pumping power. This increase is minimum for MC-BWTR and maximum for MC-AWTR, whereas MC-SWTR is moderate. The addition of ribs improves heat transfer at the expense of an increase in the friction factor (pumping power), which is quantified in terms of η . This factor was higher than one in each case, except for MC-AWTR in $100 < Re < 200$. The η for the ribbed channel was highest for MC-SWTR followed by MC-BWTR and lowest for MC-AWTR.
- Although the heat transfer capability of MC-AWTR is superior to others, its overall performance is inferior, thereby confirming that the heat transfer coefficient is not the only criteria for modification of MC-SC. On the other hand, the overall heat transfer

enhancement of MC-SWTR was higher than any other case throughout the study, and its value was significantly high in $Re > 700$.

- Moreover, η increases with Re for each case, which confirms that the increment in Nu with Re is more significant than the increment in Δp . The highest η value of 1.6 is attained for MC-SWTR at $Re = 1000$. By contrast, the lowest value of 0.87 was achieved for MC-AWTR at $Re = 100$.

Author Contributions: Conceptualization, F.A., S.A. and K.A.; methodology, K.A., S.A, F.A. and N.H.; validation, K.A., S.A, F.A., N.H., M.A., K.G., A.V. and D.Y.P.; investigation, S.A., K.A., F.A. and N.H.; writing—original draft preparation, S.A. and F.A.; writing—review and editing, M.A., K.G, A.V. and D.Y.P. All authors have read and agreed to the published version of the manuscript.

Funding: This research received no external funding.

Institutional Review Board Statement: Not applicable.

Informed Consent Statement: Not applicable.

Data Availability Statement: The data presented in this study are available upon request.

Acknowledgments: The authors acknowledge the support of UET Peshawar and Air University, Islamabad, for providing the computational facilities to conduct this research study.

Conflicts of Interest: The authors declare no conflict of interest.

Nomenclature

MCHS	Microchannel heat sink
MC-AWTR	All wall trefoil ribbed microchannel
MC-AWSR	Side wall trefoil ribbed microchannel
MC-AWBR	Base wall trefoil ribbed microchannel
Re	Reynolds number
Nu	Nusselt number
f	Friction factor
L	Length of the MCHS (mm)
H_{ch}	Height of the channel (mm)
W_{ch}	Width of the channel (mm)
D_h	Hydraulic diameter (mm)
ΔT	Temperature difference (K)
Δp	Pressure drop (Pa)
q_w	Wall flux (W/cm^2)
C_p	Specific heat capacity at constant pressure ($J/kg K$)
μ	Dynamic viscosity (kg/ms)
k	Thermal conductivity (W/mK)
ρ	Density (kg/m^3)
η	Thermal enhancement factor

References

1. Xu, M.; Lu, H.; Gong, L.; Chai, J.C.; Duan, X. Parametric numerical study of the flow and heat transfer in microchannel with dimples. *Int. Commun. Heat Mass Transf.* **2016**, *76*, 348–357. [[CrossRef](#)]
2. Tuckerman, D.B.; Pease, R.F.W. High-performance heat sinking for VLSI. *IEEE Electron Device Lett.* **1981**, *2*, 126–129. [[CrossRef](#)]
3. Ahmad, F.; Cheema, T.A.; Ur Rehman, M.M.; Abbas, A.; Woo Park, C. Thermal enhancement of microchannel heat sink using rib surface refinements. *Numer. Heat Transf. Part A Appl.* **2019**, *76*, 851–870. [[CrossRef](#)]
4. Liu, X.; Yu, J. Numerical study on performances of mini-channel heat sinks with non-uniform inlets. *Appl. Therm. Eng.* **2016**, *93*, 856–864. [[CrossRef](#)]
5. Rehman, M.M.U.; Cheema, T.A.; Ahmad, F.; Khan, M.; Abbas, A. Thermodynamic Assessment of Microchannel Heat Sinks with Novel Sidewall Ribs. *J. Thermophys. Heat Transf.* **2020**, *34*, 243–254. [[CrossRef](#)]
6. Ali, S.; Ahmad, F.; Hassan, M.; Rehman, Z.; Wadood, A.; Ahmad, K.; Park, H. Thermo-fluid Characteristics of Microchannel Heat Sink with Multi-configuration NACA 2412 Hydrofoil Ribs. *IEEE Access* **2021**, *9*, 128407–128416. [[CrossRef](#)]

7. Rehman, M.M.U.; Cheema, T.A.; Ahmad, F.; Abbas, A.; Malik, M.S. Numerical investigation of heat transfer enhancement and fluid flow characteristics in a microchannel heat sink with different wall/design configurations of protrusions/dimples. *Heat Mass Transf.* **2020**, *56*, 239–255. [[CrossRef](#)]
8. Zhu, Q.; Chang, K.; Chen, J.; Zhang, X.; Xia, H.; Zhang, H.; Wang, H.; Li, H.; Jin, Y. Characteristics of heat transfer and fluid flow in microchannel heat sinks with rectangular grooves and different shaped ribs. *Alex. Eng. J.* **2020**, *59*, 4593–4609. [[CrossRef](#)]
9. Xiao, H.; Liu, Z.; Liu, W. Turbulent heat transfer enhancement in the mini-channel by enhancing the original flow pattern with v-ribs. *Int. J. Heat Mass Transf.* **2020**, *163*, 120378. [[CrossRef](#)]
10. Hassani, S.M.; Khoshvaght-Aliabadi, M.; Mazloumi, S.H.; Rehman, S.; Alimoradi, A. Improving thermal performance of microchannels by combining rectangular pin with chamber. *Appl. Therm. Eng.* **2021**, *186*, 116373. [[CrossRef](#)]
11. Ahmad, F.; Cheema, T.A.; Mohib Ur Rehman, M.; Ilyas, M.; Park, C.W. Thermodynamic analysis of microchannel heat sink with cylindrical ribs and cavities. *J. Heat Transf.* **2020**, *142*, 092503. [[CrossRef](#)]
12. Yang, D.; Jin, Z.; Wang, Y.; Ding, G.; Wang, G. Heat removal capacity of laminar coolant flow in a micro channel heat sink with different pin fins. *Int. J. Heat Mass Transf.* **2017**, *113*, 366–372. [[CrossRef](#)]
13. Naqiuddin, N.H.; Saw, L.H.; Yew, M.C.; Yusof, F.; Ng, T.C.; Yew, M.K. Overview of micro-channel design for high heat flux application. *Renew. Sustain. Energy Rev.* **2018**, *82*, 901–914. [[CrossRef](#)]
14. Wang, G.; Chen, T.; Tian, M.; Ding, G. Fluid and heat transfer characteristics of microchannel heat sink with truncated rib on sidewall. *Int. J. Heat Mass Transf.* **2020**, *148*, 119142. [[CrossRef](#)]
15. Chuan, L.; Wang, X.D.; Wang, T.H.; Yan, W.M. Fluid flow and heat transfer in microchannel heat sink based on porous fin design concept. *Int. Commun. Heat Mass Transf.* **2015**, *65*, 52–57. [[CrossRef](#)]
16. Wang, T.H.; Wu, H.C.; Meng, J.H.; Yan, W.M. Optimization of a double-layered microchannel heat sink with semi-porous-ribs by multi-objective genetic algorithm. *Int. J. Heat Mass Transf.* **2020**, *149*, 119217. [[CrossRef](#)]
17. Ahmad, F.; Cheema, T.A.; Khan, A.; Mohib-Ur-Rehman, M.; Yildizhan, H. Hydrothermal Investigation of the Performance of Microchannel Heat Sink with Ribs Employed on Side Walls. *J. Non-Equilib. Thermodyn.* **2021**. [[CrossRef](#)]
18. Moradikazerouni, A.; Afrand, M.; Alsarraf, J.; Mahian, O.; Wongwises, S.; Tran, M.D. Comparison of the effect of five different entrance channel shapes of a micro-channel heat sink in forced convection with application to cooling a supercomputer circuit board. *Appl. Therm. Eng.* **2019**, *150*, 1078–1089. [[CrossRef](#)]
19. Karwa, R.; Sharma, C.; Karwa, N. Performance evaluation criterion at equal pumping power for enhanced performance heat transfer surfaces. *J. Sol. Energy* **2013**, *37*, 23–32. [[CrossRef](#)]
20. Steinke, M.E.; Kandlikar, S.G. Single-phase liquid friction factors in microchannels. *Int. J. Therm. Sci.* **2006**, *45*, 1073–1083. [[CrossRef](#)]
21. Wang, G.; Niu, D.; Xie, F.; Wang, Y.; Zhao, X.; Ding, G. Experimental and numerical investigation of a microchannel heat sink (MCHS) with micro-scale ribs and grooves for chip cooling. *Appl. Therm. Eng.* **2015**, *85*, 61–70. [[CrossRef](#)]